

Heat transport measurements in turbulent rotating Rayleigh-Bénard convection

Yuanming Liu ^{†1,2} and Robert E. Ecke^{1,2}

¹*Center for Nonlinear Studies*

²*Condensed Matter and Thermal Physics Group*

Los Alamos National Laboratory, Los Alamos, NM 87545

We present experimental heat transport measurements of turbulent Rayleigh-Bénard convection with rotation about a vertical axis. The fluid, water with Prandtl number (σ) about 6, was confined in a cell which had a square cross section of $7.3 \text{ cm} \times 7.3 \text{ cm}$ and a height of 9.4 cm . Heat transport was measured for Rayleigh numbers $2 \times 10^5 < \text{Ra} < 5 \times 10^8$ and Taylor numbers $0 < \text{Ta} < 5 \times 10^9$. We show the variation of normalized heat transport, the Nusselt number, at fixed dimensional rotation rate Ω_D , at fixed Ra varying Ta, at fixed Ta varying Ra, and at fixed Rossby number Ro. The scaling of heat transport in the range 10^7 to about 10^9 is roughly 0.29 with a Ro dependent coefficient or equivalently is also well fit by a combination of power laws of the form $a \text{Ra}^{1/5} + b \text{Ra}^{1/3}$. The range of Ra is not sufficient to differentiate single power law or combined power law scaling. The overall impact of rotation on heat transport in turbulent convection is assessed.

PACS numbers: 47.27.te, 47.32.Ef, 47.55.P-

I. INTRODUCTION

Turbulent thermal convection plays a key role in many of the phenomena associated with geophysical and astrophysical fluid dynamics [1] as well as providing a well-posed problem for the study of fundamental fluid dynamics [2]. In several important examples including oceanic deep convection [1] and convection in stars [3] and giant planets [4], the effects of rotation are critical in determining the nature of the fluid motion. Rotation also provides an additional parameter for understanding the origin of heat transport scaling in turbulent convection, a topic of tremendous experimental activity in recent years [2, 5]. In comparison, the research efforts applied to rotating turbulent convection have been rather modest arising from the pioneering theoretical work of Chandrasekhar [6, 7]. Experimental measurements of heat transport in rotating convection include the seminal work of Rossby [8] and later studies that also had qualitative flow visualization [9]. Numerical simulations have also had significant impact [10, 11, 12, 13, 14]. Here we consider both rotating and non-rotating convection and provide new insights into heat transport scaling of rotating convective turbulence. A short report of some aspects of this work appeared previously [15], and further studies of velocity fields in rotating convection motivated by this work were also published [16].

Rotating Rayleigh-Bénard convection can be characterized by three dimensionless parameters: the Rayleigh number Ra which is a measure of buoyant forcing, the Taylor number Ta which measures the effect of the rotational Coriolis force, and the Prandtl number σ which determines the dominant nonlinearity in convection. These parameters are defined by:

$$\text{Ra} = \frac{g\alpha d^3 \Delta T}{\nu\kappa}, \quad \text{Ta} = \left(\frac{2\Omega_D d^2}{\nu} \right)^2, \quad \sigma = \frac{\nu}{\kappa} \quad (1)$$

where g is the acceleration of gravity, α is the thermal expansion coefficient, ΔT is the temperature difference across the fluid layer of height d , ν is the kinematic viscosity, κ is the thermal diffusivity, and Ω_D is the physical angular rotation rate. The dimensionless rotation frequency $\Omega = \Omega_D d^2 / \nu$ is sometimes used in place of Ω_D or Ta. Properties of thermal turbulence can also be affected by the cell geometry characterized by the ratio of a lateral length to a vertical length. For our square geometry, we define the cell aspect ratio as $\Gamma \equiv l/d$ where l is the lateral size of the cell.

Although Ra, Ta, σ and Γ completely define the parameter space of rotating convection, the behavior of different quantities such as heat transport is complicated when one parameter is varied while keeping the others constant. For example, as Ra is increased at fixed Ta, the relative influence of buoyancy and rotation changes, making an evaluation of the influence of rotation alone difficult. To ease this problem, it is useful to define [13] an additional parameter, the convective Rossby number Ro

$$\text{Ro} = \sqrt{\frac{\text{Ra}}{\sigma \text{Ta}}} \quad (2)$$

which is a measure of a characteristic buoyant velocity to a rotational velocity. This definition is equivalent to those used previously [11, 17] and is closely related to other definitions of convective Rossby number [10, 18, 19]. Roughly

speaking, the border between rotation-dominated and buoyancy-dominated flows should be approximated by the condition $Ro = 1$.

The quantity of interest here is turbulent heat transport as measured by the Nusselt number Nu , the total heat transported by convection normalized by the heat transported by molecular diffusion alone. To appreciate the influence of rotation on Nu , it is important to understand the dependence of Nu on Ra without rotation. The investigation of non-rotating convection has been extensive over almost 40 years with early work focused on classical theories [20, 21, 22] that predicted a power law relationship of the form $Nu = A Ra^\beta$ with $\beta = 1/3$. Later measurements, particularly those in helium gas, suggested a value $\beta = 2/7$ with theory and early numerical simulations providing a solid basis for such a law. A detailed review of these results was presented by Siggia [2]. An extension [23, 24] of the competing kinetic and thermal boundary layer theory [25] that included an expanded analysis of competing boundary and bulk dissipation processes produced a phase diagram with crossover effects between different regions. Such an approach suggested a form $Nu = a Ra^{\beta_1} + b Ra^{\beta_2}$ with specific predictions for the coefficients derived from fitting a few data sets in each region. In this latter regard, high precision experimental data for room temperature fluids [26, 27] have been extremely valuable in elucidating differences between a single power law description and one involving two power laws with fixed coefficients. The measurements presented here are over a modest range of $Ra < 10^9$, and thus cannot distinguish between these two forms. We compare our results with a broad range of measurements of heat transport of non-rotating convection as a benchmark for considering the effects of rotation on turbulent heat transport.

The effects of rotation on convection, especially on heat transport, might be expected to be substantial given that rotation profoundly changes the nature of boundary layer instability and modifies the length scales over which motions occur. Whereas thermal plumes are formed in long sheets and are swept across the cell by mean flow, rotation spins up these plumes into intense vortical structures. Furthermore, rotation is known to shorten the linear length scale dramatically as rotation is increased [7]. Additional ingredients introduced by rotation are the Ekman pumping/suction imposed by the differential rotation of the boundary and the interior flow and the dynamical constraints imposed by the Taylor-Proudman Theorem for strongly rotating flows. Despite these interesting factors, previous heat transport measurements have not been well understood for a number of reasons. Rossby, in his seminal paper on rotating convection [8], reported comprehensive heat transport for water and for mercury as function of Ra and Ta with emphasis on the regions close to onset and of moderate Ra ($< 3 \times 10^6$). His measurements, as well as later measurements in helium [28], quantitatively showed that the convective onset was below the theoretical prediction of linear stability analysis [6, 7]. This reduction in critical Rayleigh number was attributed to a transition to azimuthally-periodic modes localized near the wall [28, 29] but neither of the experiments had flow visualization capabilities. The existence of such wall states was later confirmed [9, 30] using shadowgraph flow visualization but rather than being stationary the sidewall states were observed to precess in the rotating frame counter to the direction of rotation. This resolved one difficulty with the data set of Rossby.

Other experiments [18, 31, 32] and numerical simulations [10, 12, 19] of rotating convection involve an open upper fluid surface where one can visualize the development of convective structures and the interaction of vortices and characterize some of the statistics of the temperature and velocity fields. These experiments are, however, not amenable to the measurement of accurate heat transport.

The heat transport experiments [9] that motivated this work used a water in a cylindrical cell with top and bottom rigid boundaries, and measurements were made to higher Ra ($\approx 2 \times 10^7$) than Rossby. The normalized heat transport Nu at constant rotation rate appeared, however, to asymptote to the non-rotating result at high Ra . This combination of rather small Ra and an apparently non power-law scaling was confusing. Numerical simulations [14] showed, however, that Nu scaled approximately as the $2/7$ power for a fixed convective Rossby number with no-slip top and bottom boundary conditions. To test this prediction and to further characterize heat transport as a function of rotation, it was necessary to extend the heat transport measurements to higher Ra than in [9]. Single point measurements of temperature made in the same cell as the one used here will be presented elsewhere.

This paper is organized as follows. The experimental apparatus and procedures are described in Sec. II. The heat transport results of non-rotating and rotating turbulence are presented in Sec. III and Sec. IV, respectively. Sec. V summarizes the paper.

II. EXPERIMENTAL PROCEDURE

A. Rotating apparatus and cell

The experimental apparatus, shown schematically in Fig. 1, was an improved version of the one used previously in studies of rotating convection [9, 33]. The top plate temperature of the cell was controlled by water flow which was distributed evenly by a set of 12 turrets divided into two groups pointing to $1/3$ and $2/3$ of the radius, respectively.

The water flow was temperature-controlled by a refrigerator-circulator and then fed into the rotating frame through

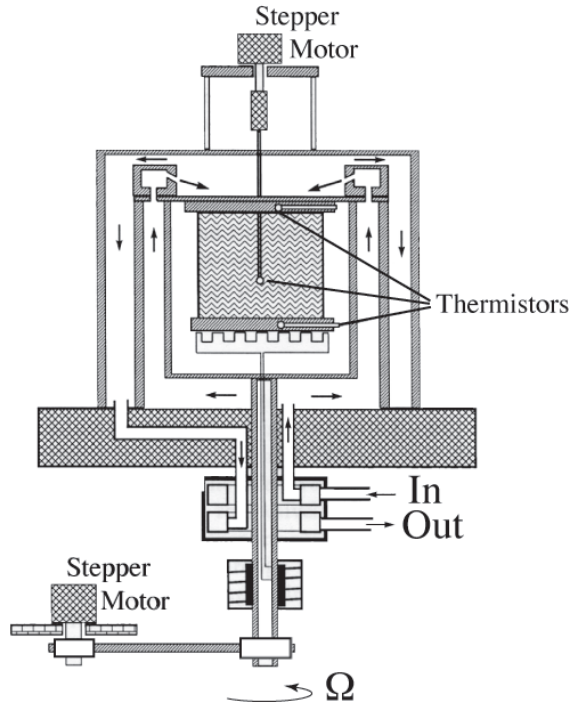


FIG. 1: Schematic of the experimental apparatus

a water slip connection. The flow was further temperature regulated by a feedback temperature control unit which maintained the top-plate temperature constant with r.m.s. fluctuations of less than 1 mK. A film heater attached to the bottom plate provided a constant heat current to the fluid layer. The power input was obtained by measuring the voltage across the film heater and the current through it. The latter was obtained from the voltage across a temperature-controlled standard resistor.

All electrical wires were fed into the rotating frame through an electrical slip ring and inside a hollowed steel shaft which also served as the drive train for rotation. The electrical noise of the slip ring was small enough that there was no measurable difference in the signals with or without rotation. Rotation was provided by a micro-stepping motor through a shaft, two gears and a timing belt and was under computer control. The gear ratio set a lower limit for the frequency of about 0.01 Hz. The maximum frequency surveyed was 0.5 Hz.

The convection cell was constructed with aluminum top (1.27 cm thick) and bottom (0.64 cm thick) plates and plexiglass sidewalls (0.32 cm thick). The aluminum plates were anodized to prevent corrosion in water. The cell had a height $d = 9.40$ cm and horizontal dimensions $L_x = L_y = 7.30$ cm with an aspect ratio of $\Gamma = L_x/d = 0.78$. The cell's bottom and sides were insulated by 2.5-cm-thick styrofoam to reduce thermal losses from radiation and conduction or convection by air. Four thermistors were embedded in each of the top and bottom plates and the thermistor centers were located at 0.32 and 0.23 cm from the fluid, respectively, and at the mid point between the cell's center and the sides. The four thermistors in each plate gave the average plate temperature. The wires from the film heater and from the four thermistors were heat sunk on the bottom of the cylindrical can which was maintained at the same temperature as the top plate.

B. Heat Transport

Heat is transported more efficiently by convection where heat can be advected by the fluid motion than by conduction where heat is transported solely by diffusion. The enhancement of thermal transport by convection is characterized by the Nusselt number $Nu = K_{eff}/K$ where K_{eff} and K are the effective thermal conductance and molecular thermal

conductance of the fluid layer, respectively. In an experimental realization of convection there are additional heat transport contributions to the measured thermal conductance. These include conduction through the cell sidewalls and from conduction, convection, and radiation to the surrounding environment. Below the onset of convection, the background conductivity can be measured and effectively subtracted from the total heat transport contribution provided that the thermal conductivity of water, available from the literature, is assumed. For turbulent convection in room temperature experiments this is difficult to accomplish because if $\Delta T \approx 10K$ corresponds to the maximum $Ra \approx 10^9$ then the onset of convection occurs for $\Delta T \approx 2 \times 10^{-5}K$, far below experimental resolution. This can be overcome by rotating the cell, thereby suppressing the onset of convection by about four orders of magnitude, *i.e.*, $\delta T \approx 0.2K$, and allowing the background thermal conductivity to be measured directly. We now describe this procedure in detail.

The background thermal conductance was determined to be $K_b = 0.0423 \pm 0.0004$ W/K, comparable to the water layer's thermal conductance $K = 0.0341$ W/K at a cell mean temperature of 21.5 °C. Assuming that K_b is independent of the mean temperature of the cell, the Nusselt number is given by

$$Nu = \frac{\dot{Q}/\Delta T - K_b}{K}, \quad (3)$$

where $\Delta T = T_b - T_t$ is the temperature difference across the water layer with T_t and T_b being the top-plate and bottom-plate temperatures, \dot{Q} is the total heat input to the bottom plate, and K is the thermal conductance of the water layer at the mean temperature $T_0 = (T_t + T_b)/2$. The top and bottom temperatures are corrected for the temperature drop in the aluminum plates although this correction was always less than 0.3%.

In our experiment, we measured K_b at a single temperature because the temperature dependence of the background terms is quite small and does not affect the data presented here. To evaluate the systematic error in our measurements of K_b , we have estimated the different contributions in that quantity. The major contributors to K_b are the plexiglass side walls, the insulating foam, the electrical wires, and thermal radiation. The first three contributions have very weak temperature dependence (less than 1% change over a 20 K temperature difference) and small magnitude, estimated to be 0.006, 0.006, and 0.003 W/K, respectively. The rest of the measured background heat transport, about 60% of K_b (≈ 0.027 W/K), comes from a series combination of conduction through the foam, convection in the air surrounding the insulation, and from thermal radiation from the outer surfaces of the insulation to the surroundings which are maintained at the top-plate temperature. The top-plate temperature was held constant and the bottom-plate temperature was changed by a maximum of 20 K corresponding to the maximum heat input. This produces about a 2 K increase in the average temperature of the radiating surfaces, or about a 2% increase in radiated heat, which results in about a 0.02 overestimate in Nu. Therefore, for the measurements with fixed T_t , K_b can be taken to be constant as the correction to Nu is less than 0.1%.

This analysis neglects an important point regarding the heat transported through the side walls [34]. Rather than supporting a linear temperature profile as in the non-convecting state where the background is measured, the side walls are in contact with a turbulent fluid that is approximately iso-thermal in the bulk of the flow. This leads to an enhancement of heat transport through the side walls in the turbulent state. For conditions similar to those presented here (thin plexiglass walls relative to the lateral extent of the system), however, the correction to the total heat transport was shown by numerical modeling to be small, ranging from about 2% for $Nu = 10$ to 1% at $Nu = 100$. Our sidewall is thicker by about a factor of two, so in the worst case these values might be twice as large. Applying a correction of this order shifts the exponent of a power law fit by at most 1% (higher) and the constant term by about 7% (lower). These estimates contribute to the systematic error in our results but we do not explicitly correct for the side wall effect in the data presented below.

C. Parameter space

The parameter space for rotating convection is defined by Ra and Ta (or Ω) which are proportional to the physical control variables of ΔT and Ω_D , respectively. In Fig. 2, the parameter space is shown over a range which encompasses our experimental measurements. The shaded region denotes the area in which most of our efforts were focused. The limitations which determine that area are the range of measurable ΔT for a given cell height d ; a four-decade variation of Ra was obtained by varying the temperature difference across the cell from 2 mK to 20 K. The Taylor number for the shaded area ranged from about 1×10^6 to 5×10^9 , corresponding to rotation frequencies from $f = 0.01$ Hz to 0.5 Hz. The lower limit was determined by the range of stability of the stepping motor given a particular gear ratio. By reducing that ratio, lower Taylor numbers could have been investigated but this proved unnecessary as the interesting range of Ta was spanned with the chosen gear ratio.

During the experiments, we fixed some parameters and studied the dependence of measured quantities on the others. For instance, we fixed Ra to study the dependence on Ta , and *visa versa*. One important parameter, the

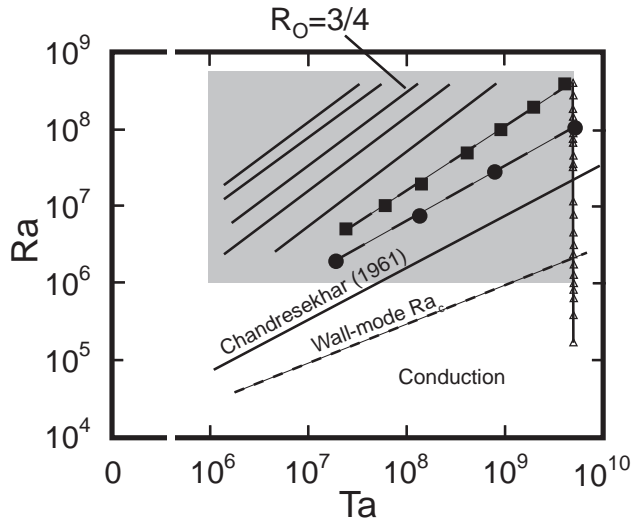


FIG. 2: Parameter space of Ra vs Ta . Most measurements were conducted in the gray area by fixing Ra , Ω_D , or Ro . The measurements at $\Omega_D = 0.0$ Hz and 3.14 Hz ($Ta \approx 5.0 \times 10^9$) started at Ra as low as 5×10^5 . Five solid lines in the gray area represent five different Ro (from right to left, 0.30, 0.52, 0.75, 1.15, and 1.49) used in the measurements. Data (●), from heat transport measurements at constant Ω_D , set the lower bound of Ra above which Nu could be expected to exhibit turbulent convection. Symbols (■), deduced from Nu data at fixed Ra , represent the loci of maximum Nu at constant Ra . The data (△) at the highest $Ta \approx 5 \times 10^9$ spanned the largest Ra number range. The theoretical prediction of convective onset under rotation [7] is also shown in the figure.

convective Rossby number Ro which provides a relative measure of buoyancy relative to rotation, was maintained fixed by varying both ΔT and Ω_D for each data point. The contours of constant Ro , plotted in Fig. 2, are approximately straight lines in the log-log plot. Numerical simulations of turbulent rotating convection with $\sigma = 1$ [13, 14] followed the contour of $Ro = 3/4$ where buoyancy and rotation had roughly comparable importance. This particular line is noted in the figure. Several other sets of data shown in the figure are discussed later. Overall, the parameter ranges in our experiments fall roughly into the region studied in open-top experiments [18, 31, 32]; the parameter space of experiments on rotating convection prior to about 1990 was summarized in [18]. (the *flux* Rayleigh number used in that parameter space is related to Ra by $Ra_f = NuRa$ so that the highest Ra in our experiments, where $Nu \approx 60$ corresponds to $Ra_f \approx 3 \times 10^{10}$).

III. HEAT TRANSPORT IN NON-ROTATING CONVECTION

In this section, we present experimental results for non-rotating convection. This enables us to compare our results with existing theories and with other non-rotating convection experiments, of which there are many. It also serves as a reference for our results on rotating convection. We concentrate here on measurements of heat transport in fluids with Prandtl number $\sigma \approx 6$.

Heat transport is measured by the Nusselt number Nu and scales with Ra as a power-law: $Nu = ARa^\beta$. Classical arguments [20, 21] suggest $\beta = 1/3$ whereas other scaling theories [25, 35] predict $\beta = 2/7$. Another approach that generalizes the latter theories [23] predicts a complicated phase diagram as a function of Ra and σ . In different regions different power-law scalings dominate with strong crossover effects so that one obtains a form for the heat transport where Nu scales with Ra as $aRa^{\beta_1} + bRa^{\beta_2}$ with β_1 and β_2 fixed. Careful heat transport measurements have demonstrated that this latter prediction yields better fits to experimental data [26]. For the limited range of Ra presented here, either approach yields a good fit to the data.

The Nusselt number of non-rotating convection measured with fixed T_t is shown in Fig. 3 as a function of Ra for $4 \times 10^6 < Ra < 5 \times 10^8$. The results are reasonably well described by a power-law with scaling coefficients $A = 0.158 \pm 0.003$ and $\beta = 0.289 \pm 0.002$ which were obtained by fitting all data for $4 \times 10^6 < Ra < 5 \times 10^8$ shown in the figure. Fitting the data between 4×10^7 and 5×10^8 yields slightly different values: $A = 0.164 \pm 0.003$ and $\beta = 0.286 \pm 0.002$. These latter values have the virtue of being derived from a range of Ra which is in the turbulence

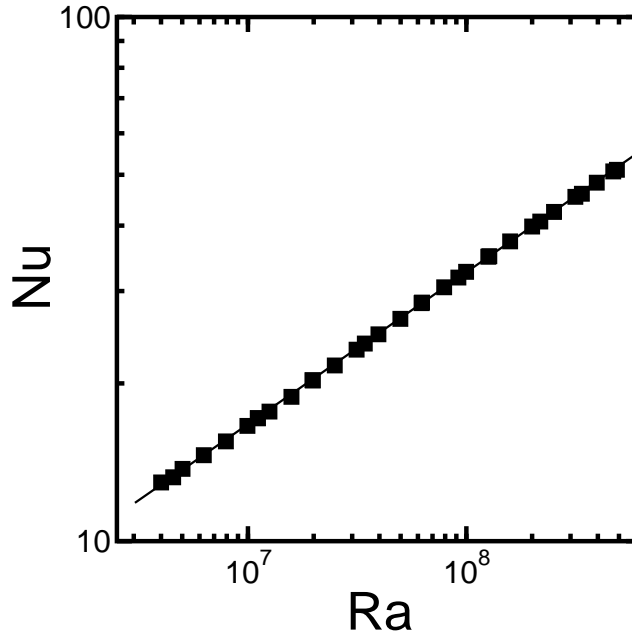


FIG. 3: Nu vs Ra for non-rotating convection. The solid line is the power-law fit $\text{Nu} = 0.158 \text{Ra}^{0.289}$ over the range $4 \times 10^6 < \text{Ra} < 5 \times 10^8$. An equivalent fit is $\text{Nu} = 0.262 \text{Ra}^{1/5} + 0.0473 \text{Ra}^{1/3}$.

| A | β | $A_{2/7}$ (10^7) | $A_{2/7}$ (10^8) | Ra Range ($\times 10^6$) | Γ | Reference |
|----------|----------|-------------------------|-------------------------|-------------------------------|----------------------|-------------------------------|
| 0.131 | 0.300(5) | 0.165 | 0.170 | 0.03 – 2 | 2.8-10 (C) | Rossby (1969) |
| 0.183 | 0.278 | 0.162 | 0.159 | 0.3 – 100 | 1.5×2.5 (R) | Chu & Goldstein (1973) |
| 0.145 | 0.29 | 0.155 | 0.156 | 30 – 4000 | 3.5-14 (S) | Tanaka & Miyata (1980) |
| 0.137 | 0.275(7) | 0.115 | 0.112 | 2 – 200 | 0.71, 1.6 (S) | Solomon & Gollub (1991) |
| 0.129 | 0.299(3) | 0.160 | 0.164 | 0.1 – 20 | 2.0 (C) | Zhong <i>et al.</i> (1993) |
| 0.19(4) | 0.28(1) | 0.172 | 0.170 | 1 – 400 | 4×1 (R) | Chillá <i>et al.</i> (1993) |
| 0.145 | 0.292 | 0.160 | 0.162 | 400 – 7000 | 1.0 (C) | Cioni <i>et al.</i> (1996) |
| 0.16 | 0.281(2) | 0.147 | 0.145 | 800 – 6000 | 1.0 (C) | Shen <i>et al.</i> (1996) |
| 0.164(6) | 0.286(3) | 0.164 | 0.164 | 40 – 500 | 0.78 (S) | This work |
| 0.154 | 0.291 | 0.168 | 0.170 | 3000-60000 | 1.0 (C) | Nikolaenko and Ahlers (2003). |

TABLE I: Values of heat transport scaling parameters: A , β , $A_{2/7}$ ($\text{Ra} = 10^7$), $A_{2/7}$ ($\text{Ra} = 10^8$), Ra-Range, Γ (C: cylindrical with Γ =diameter/height, S: square with Γ =width/height, R: rectangular with $\Gamma_x \times \Gamma_y$), and reference. All the experiments listed here used water as the working fluid. The Prandtl number for different experimental conditions varied slightly but was in the range $4 < \sigma < 7$.

regime but with the disadvantage of a shorter scaling range. To account for this systematic uncertainty we take $A = 0.164 \pm 0.006$ and $\beta = 0.286 \pm 0.003$ as the best estimates for the scaling coefficients. The exponent is very close to $2/7$ and agrees well with earlier work as summarized in Table I. Although the $2/7$ value has been shown not to describe heat transport data over a much larger range of Ra [26], we use it here for convenience. Further, the uncertainties associated with the exponents and coefficients are the result of statistical fits and almost certainly underestimate the systematic errors associated with the different experiments.

Compared to the scaling exponent β , the coefficient A is quite different from one experiment to another. A is sensitive to the exponent and a precise determination of A requires a larger range of Ra than has been available in any of the experiments using water. Fixing the exponent at $2/7$ and computing a value for $A_{2/7}$ (equivalent to $\text{Nu}/\text{Ra}^{2/7}$) at different Ra gives a better comparison between data sets, see Table I. For the water experiments and for $10^7 < \text{Ra} < 10^9$, the coefficients agree quite well except for the experiments of Solomon and Gollub [36] where a liquid

mercury bottom surface may account for the discrepancy. All of the data reported earlier and listed in the Table do not directly measure the background heat transport contribution that we are able to account for using rotation. This background measurement is important in eliminating systematic error for smaller Nu. An average over all the data sets for convection in water yields $A = 0.161 \pm 0.007$ and $\beta = 0.287 \pm 0.008$ with no statistically-significant dependence of Nu on Γ . In summary, our data for non-rotating convection agree well with earlier results despite the significant variation in aspect ratios between experiments.

We also took heat transport data at fixed mean-cell temperature T_0 to estimate the Prandtl number dependence of the heat transport [15] (not reported here). We can use that data to correct the data at fixed T_t . In the fixed T_t measurements reported in the remainder of this paper, we had a variation in the range $21.5^\circ\text{C} < T_0 < 31.4^\circ\text{C}$ (and resultant $6.7 > \sigma > 5.2$) corresponding to changes from the lowest to highest heat input. Such non-constant σ or T_0 results in an uncertainty in Nu of the order of 0.8%. We interpolate the Nu data to a constant mean temperature or a constant σ . We choose $T_0 = 26.0^\circ\text{C}$ (where $\sigma = 5.93$) as the reference temperature which was about the average of the mean temperatures in the experiments. The interpolated value is given by $\text{Nu} = \text{Nu}_m (\sigma/5.93)^{0.0292}$ where Nu_m is the measured Nusselt number using Eq. 3. The difference between the interpolated and measured values of Nu is less than 0.8%, and does not change the scaling coefficients within their specified error bars. Nevertheless, the interpolated values are reported in Fig. 3.

One important feature of turbulent convection is the large scale circulation that is driven by an accumulation of thermal plumes that congregate near the lateral boundaries [2, 5]. The general circulation in our cell was visualized using glass encapsulated thermochromic liquid crystals (TLC). A white light sheet about 1mm in width was used to illuminate the cell from the side and a black background was provided for good contrast. The mean-flow direction was typically across the cell diagonal. Flow reversals were observed as was a shifting of the main diagonal circulation in a clockwise or counterclockwise direction as viewed from above. This meant that sometimes the flow along the off-diagonal direction reversed directions frequently. This cross diagonal flow has been observed before in convection cells with square cross section [36]. In addition to the large diagonal flows there were often small recirculating cells in the corners and along the bottom-side boundary. Viewed from above the thermal plumes near the bottom boundary layer were arranged into coherent sheets which were swept up by the mean flow. This was also seen in a number of convection experiments in water where the flow is easy to visualize [36, 37, 38].

IV. HEAT TRANSPORT IN ROTATING CONVECTION

Heat transport measurements in the presence of rotation are complicated by the changing influences of buoyancy, proportional to Ra, and rotation, proportional to Ω_D . The simplest thing to do experimentally is to fix Ω_D and vary ΔT . Because the mean temperature changes with ΔT (fixed T_t), the dimensionless Ω changes owing to the temperature-dependent viscosity of water. This can be as large as 25% over the Ra range that we studied. As noted above σ also changes somewhat but that influence is small. Even constant Ω is not the appropriate variable to hold constant if one wants to evaluate the behavior of Nu as a function of Ra for a constant rotational forcing. From previous heat transport measurements [9], it appeared that Nu at fixed Ω_D was enhanced by rotation for intermediate Ra but seemed to asymptote to the non-rotating value of Nu at higher Ra. A convenient measure of rotational forcing [13, 14] is defined by the ‘‘convective’’ Rossby number, $\text{Ro} \equiv \sqrt{\text{Ra}/(\sigma\text{Ta})}$, which is the ratio of a rotational period to a buoyancy time. So $\text{Ro} \approx 1$ should mark the border between strongly rotating convection with $\text{Ro} \ll 1$ and weakly rotating convection with $\text{Ro} \gg 1$. In those numerical simulations of rotating convection at fixed $\text{Ro} = 0.75$, Nu scaled approximately as $\text{Ra}^{2/7}$. Here we present heat transport measurements to higher Ra than previously [9] and consider Nu as a function of Ra at fixed Ro. In addition, we compare our results to earlier ones by Rossby [8] who compiled constant Nu contours as a function of Ra and Ta. To get a good understanding of the whole system, it is useful to consider different slices of the parameter space. We present them in the order of contours of Nu, fixed Ω_D , fixed Ra, and finally fixed Ro.

Heat transport measurements in rotating convection can be summarized by a contour plot of Nu presented in Fig. 4. The points on each constant-Nu line were obtained by interpolating Nu data measured under different controlled conditions (namely, fixed Ω_D , Ra, and Ro). The individual data points are within 1% of the smooth curves for large Nu and within 3% for the smallest Nu. Figure 4 complements the Nu contour plot in Fig. 11 of Rossby [8] where the highest Nu was 12, and the combination of the two gives a rather complete description of Nu in the parameter space of $\text{Ra}_c \leq \text{Ra} < 10^9$ and $0 \leq \text{Ta} < 10^{10}$. As shown in Fig. 11 of [8] for the lower Ra and Ta range, there is a minimum Ra for constant Nu or alternately there is a maximum Nu at constant Ra. At fixed Ta, however, Nu is a monotonically increasing function of Ra. In the following, results are presented which elucidate the origin of the maximum Nu at fixed Ra (or the minimum Ra at fixed Nu) and investigate the variation of Nu as a function of Ra, Ta, and Ro. Before proceeding with these details, however, we can already see the overall trend of heat transport at fixed Ra. For low rotation, Nu is rather insensitive to changes in Ta (note the discontinuity in the horizontal axis in

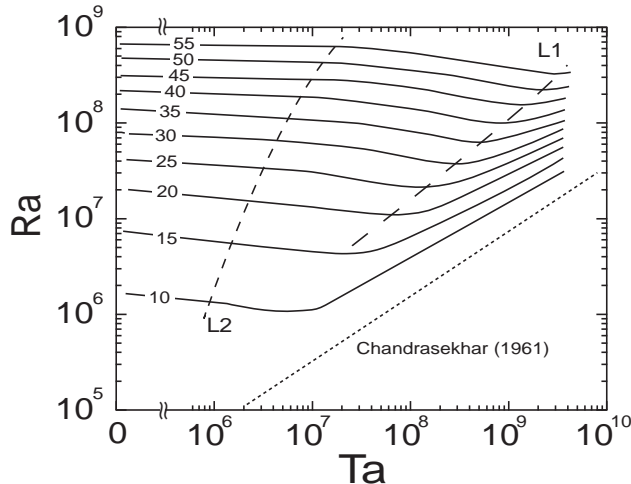


FIG. 4: Lines of constant Nu as a function of Ra and Ta. The dotted line is for the bulk convective onset from Chandrasekhar and $Ra_c \propto Ta^{2/3}$. Line $L1$ connects the loci of maximum Nu at constant Ra and agrees well with the loci of the minimum Ra at constant Nu. Line $L2$ delimits the parameter space into the right section where we made measurements under rotation and the left section which are interpolated between zero rotation and the data with the lowest Ta.

Fig. 4). In the intermediate range between lines $L2$ and $L1$, Nu increases with increasing Ta, as rotation enhances heat transport. For high enough Ta, however, rotation suppresses convection and Nu decreases as the onset of bulk convection is approached at $Ra_c(Ta)$.

A. Constant Ω_D

Shown in Fig. 5 is Nu versus Ra at $\Omega_D = 3.14$ Hz where we obtained the background conductance K_b as described in Sec. II. The first few points have larger uncertainty because of the small temperature difference ΔT across the cell and the long thermal diffusion time in our cell (about 16 h). The transition to convection from a conduction state occurred at $\Delta T_c \approx 150$ mK and $Ra_c \approx 2 \times 10^6$, much lower than the theoretical value of 1.6×10^7 for a laterally-infinite system at this rotation rate [7]. This lower-than-expected transition was observed in early heat-transport experiments [8, 9, 28] and was later visually identified as a transition to a side-wall traveling-wave state [9, 30]. Extrapolating the results in [9] to $\Omega = 2.88 \times 10^4$, one obtains the onset to the traveling state at about 3×10^6 , not far from our value of 2×10^6 . There is also an inflection point in Nu at $Ra_b \approx 1.6 \times 10^7$, coinciding with the theoretical prediction [7] for the transition to bulk convection [9, 33]. Note that as the mean temperature of the cell increased during the measurements (constant T_t), Ω and Ta increased from 2.88×10^4 and 3.31×10^9 at small Ra to 3.58×10^4 and 5.12×10^9 at the highest Ra, respectively.

We also measured Nu at $\Omega_D = 0.00, 0.188, 0.502,$ and 1.26 Hz. These measurements, shown in Fig. 6, served as a rough characterization of the system. The first observation is that higher rotation suppresses convection relative to non-rotating convection from onset up to a value of Ra that depends on rotation. Above that Ra, Nu is higher than its corresponding value without rotation. Thus, the notion that rotation is a damping influence on convection, as suggested by the Taylor-Proudman theorem, is only valid near onset and the opposite is true for turbulent convection. The values of Ra_s for this crossover are plotted in Fig. 2 as solid circles. It is the crossover that gives rise to the maxima in the contours of Nu. The second thing to notice is that although $Nu(R, \Omega)/Nu(Ra, 0) > 1$ at intermediate Ra, it appears to asymptote to 1 at higher Ra. This suggests that buoyancy wins out over rotation at high Ra and fixed Ω .

Revisiting the presence of mean flow, a feature of non-rotating convection over a large range of Ra, we consider mean flow for rotating convection. On the one hand, flow visualization in the rotating frame for a cylindrical cell with $5 \times 10^7 < R < 5 \times 10^8$ [16] used both thermochromic liquid crystal (TLC) and particle image velocimetry to determine the flow structure near the upper boundary layer [16]). The sheet-like plumes evolved under rotation into vortices and for small enough Ro, *i.e.*, for rotation dominated flow, there was no indication of a large scale circulation extending over the size of the container. It seems that the shear on the boundary layer is of a very different form than

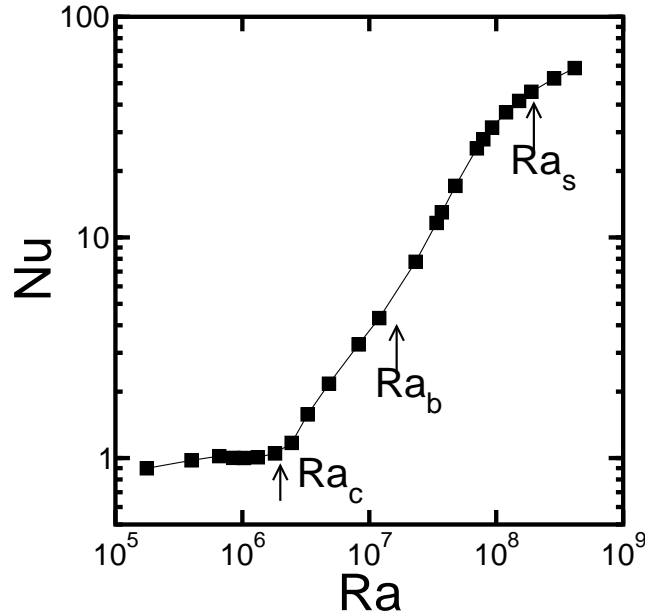


FIG. 5: Nu vs Ra for $\Omega_D = 3.14$ ($\Omega \approx 3.3 \times 10^4$). The arrows indicate the onset of the side-wall traveling state at Ra_c and the bulk state Ra_b . The approximate onset of turbulent convection is indicated as Ra_s . The line is a guide to the eye.

for non-rotating convection as strong vortical motions dominate the flow just outside the boundary layer. Results for higher Ra in the range 10^9 to 3×10^{11} [39] indicated a precessing mean flow provided $Ro > 0.5$. Similarly, recent results showed a breakdown of large-scale circulation for $Ro < 1.2$ [40].

B. Constant Ra

Another way to look at the influence of rotation on convection is to fix Ra and vary Ω . We measured Nu as a function of Ta at Rayleigh numbers of $Ra = 5 \times 10^7, 1 \times 10^8, 2 \times 10^8, 4 \times 10^8$, with results as shown in Fig. 7. For each Ra , the data were corrected so that σ was constant. We have also included data for $Ra = 2 \times 10^7, 1 \times 10^7, 5 \times 10^6$ which were obtained by interpolating data measured at constant Ro and Ω_D . For all the data sets, Nu increased with rotation before decreasing at higher Ta with a maximum Nu that varied with Ra . The loci Ta_m of maximum Nu are plotted in Fig. 2 as solid squares and in Fig. 4 (line $L1$). Note in the latter figure that this line approximately connects the loci of minimum Ra for each Nu contour. Line $L1$ can be approximated by $Ra \approx 2.2Ta^{0.85}$, differing from the relation of $Ra \approx 206Ta^{0.63}$ at lower Ra and Ta reported by Rossby (1969). The very different exponents indicate a continuously steepening curve and suggests that there is no clear asymptotic (in Ta) power-law scaling for the Nu maxima over the Ta range studied so far.

An interesting conjecture regarding the enhancement of heat transport by rotation is that rotation creates thermal vortices which increase Nu through Ekman pumping in the boundary layer [9, 14]. Thus, the enhancement in Nu might be proportional to the number of such vortices. Because we have not visualized the flow for the rotating system, the number of vortices as a function of Ta is not known directly [16, 41]. Instead we consider the linear prediction for the number of structures at the convective onset. The linear wavenumber k_c increases with Ta and asymptotically scales like $Ta^{1/6}$ [7] which implies that the number of cellular structures should scale like $k_c^2 \sim Ta^{1/3}$. This scaling for vortex number was observed even significantly above onset in experiments with an open top surface [31] which suggests it is a reasonable assumption here. Instead of the $1/3$ scaling of the asymptotic theory, however, we will compare with an empirical fit to the linear data over our range of Ta which gives $k_c(Ta)/k_c(0) \approx 0.090Ta^{0.355}$. In Fig. 8, we plot Nu in Fig. 7 as a function of $Ta^{0.36}$. For $Ta < Ta_m$, there is a linear region for each Ra that shrinks as Ra decreases. In the linear region, we have

$$Nu = Nu_0 + \gamma Ta^{0.355}, \quad (4)$$

where Nu_0 and γ are fitting parameters and values for different Ra are listed in Table II. Solid lines in Figs. 7 and

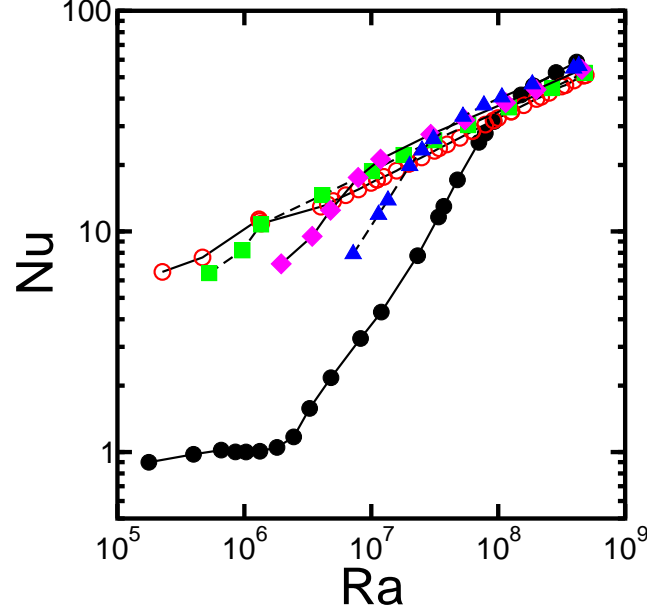


FIG. 6: (Color online) Nu vs Ra at constant Ω_D : 0.00(\circ), 0.188(\blacksquare), 0.502(\diamond), 1.26(\triangle), and 3.14(\bullet). The lines are guides to the eye.

| Ra ($\times 10^6$) | Nu_m | Ta_m ($\times 10^7$) | $Nu(\Omega_D = 0)$ | Nu_0 | γ |
|-------------------------|--------|-----------------------------|--------------------|---------|------------|
| 400 | 58.0 | 420 | 48.38 | 48.2(2) | 0.0051(5) |
| 200 | 49.0 | 200 | 39.87 | 39.5(1) | 0.0061(4) |
| 100 | 40.5 | 90 | 32.62 | 32.5(1) | 0.0065(2) |
| 50 | 33.0 | 42 | 26.60 | 26.7(1) | 0.0067(3) |
| 20 | 25.5 | 14 | 20.31 | 20.6(2) | 0.0066(4) |
| 10 | 20.5 | 6 | 16.62 | 16.9(2) | 0.0059(9) |
| 5 | 16.0 | 2.5 | 13.65 | 13.8(3) | 0.0055(12) |

TABLE II: Fitting parameters Nu_0 and γ . Nu_m and Ta_m are the maximum Nusselt number and its location at constant Ra. $Nu(\Omega_D = 0)$ is the non-rotating value obtained by cubic least-square interpolation of $\text{Log}(Nu)$ vs $\text{Log}(Ra)$ for non-rotating convection.

8 are calculated from these fitting parameters. The deviation from the solid lines (linear behavior) at higher Ta is a result of rotation suppressing convection in the weakly nonlinear regime near onset. Also listed in Table II is $Nu(\Omega_D = 0)$, the Nusselt number of non-rotating convection. The fitting parameter Nu_0 for all Ra is nearly identical to $Nu(\Omega_D = 0)$ within fitting and experimental uncertainties. This indicates that the fitting is consistent with the data in the range $0 < Ta < Ta_m$. Thus, the enhancement of Nu by rotation is given by $\Delta Nu = \gamma Ta^{0.355}$ with γ about 0.006. This result supports the conjecture that the enhancement is proportional to the average number of thermal vortices.

Using velocity field measurements [16], the number of vortices could be evaluated more quantitatively. At a fixed $Ra = 3.2 \times 10^8$, Ta was varied from 0 up to about 10^{10} . The variation of vortex (cyclonic) density with Ω was slightly sub-linear, over the range $10^7 < Ta < 10^9$. Since $\Omega \sim Ta^{1/2}$, this result suggests that the number of vortices depends on Ta with a power a bit less than 1/2. This is roughly consistent with the estimate based on linear stability arguments. Unfortunately, the vortex density data are too sparse to provide better estimates in the Ta range of interest.

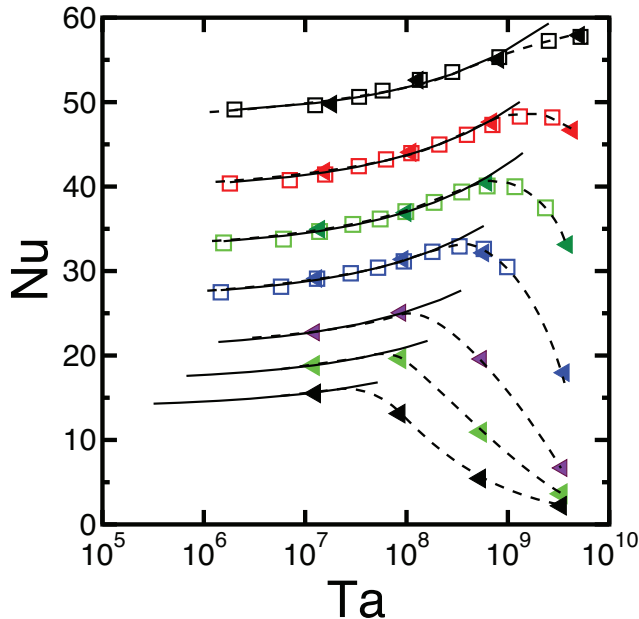


FIG. 7: (Color Online) Nu vs Ta at (from top to bottom) $Ra = 4.0 \times 10^8$, 2.0×10^8 , 1.0×10^8 , 5.0×10^7 , 2.0×10^7 , 1.0×10^7 , and 5.0×10^6 . \square – measured experimentally with Ra held fixed and \blacktriangleleft – interpolated from data measured at constant Ω_D (Fig. 6). Solid lines are least-square fits to the data; dashed lines are guides to the eye.

C. Constant Ro – power-law scaling

Many experiments in thermal convection without rotation showed that Nu scales more closely as the $2/7$ power of Ra in the regime $10^7 < Ra < 10^9$ than with the classical $1/3$ power law. As discussed earlier, a generalized theory in terms of a phase diagram in Ra and σ and more precise experimental measurements suggest a form with the sum of two power laws with exponents of $1/5$, $1/4$, $1/3$, or $1/2$ depending on the region in phase space. Rotation complicates the issue of scaling since the relative influence of rotation changes with changing Ra at fixed Ta. Numerical simulations [14] showed that the convective Rossby number is a good measure of the relative importance of buoyancy with respect to rotation: for $Ro = 0.75$ and $\sigma = 1$, $Nu \sim Ra^{2/7}$ which indicates that the details of rotation are relatively unimportant in the determination of the scaling behavior. We have tested this prediction and over the range $0.1 < Ro < 1.5$ find approximate $2/7$ power-law scaling. We use this single power law description for convenience - a fit of the form $Nu = a Ra^{1/5} + b Ra^{1/3}$ yields equivalent fits. For the non-rotating case, the coefficients are $a = 0.26$ and $b = 0.047$.

We have measured Nu at several constant Rossby numbers, i.e., $Ro = 0.12, 0.30, 0.52, 0.75, 1.15, 1.49$, and ∞ (zero rotation). For clarity, only part of the data for $Ro = 0.30, 0.75$, and infinity are plotted on a log-log scale in Fig. 9 with the coefficients of power law fits listed in the plot. The Nusselt number agrees well with a $2/7$ power law and is different from the $1/3$ power law, especially at higher Rayleigh number ($> 4 \times 10^7$). In Fig. 10, we plot $Nu/Ra^{2/7}$ versus Ra to gauge how well the $2/7$ power law describes the data. Over the Ra range where the $2/7$ power law is satisfied, a constant value of $A_{2/7} = Nu/Ra^{2/7}$ is expected. The description is reasonably good for the non-rotating case, but becomes a little worse as Ro decreases or rotation increases. The coefficient $A_{2/7}$ is plotted in Fig. 11(c). The trend of increasing $A_{2/7}$ with decreasing Ro demonstrates the enhancement of heat transport by rotation.

We also fit the data with $Nu = A_\beta Ra^\beta$ to obtain the coefficient and the exponent as functions of Ro. Least-squares fitting was performed in the range $4 \times 10^7 < Ra < 5 \times 10^8$ to avoid possible deviation from power-law scaling at lower Ra. The results are plotted in Fig. 11. It should be pointed out that for non-rotating convection the coefficient $A = 0.164$ and exponent $\beta = 0.286$ are slightly different from the values obtained by fitting the data for $4 \times 10^6 < Ra < 5 \times 10^8$. For finite Ro, the exponent depends on Ro: it decreases almost monotonically from 0.287 at $Ro = 1.5$ to 0.269 at $Ro = 0.12$. As shown in Figs. 9, 10, and 11, the coefficient A increases as rotation increases, and its value is very sensitive to the fitting value of exponent as can be seen by comparing Fig. 11(b) and (c).

Determining unambiguously the scaling behavior of the heat transport requires many orders of magnitude in Ra. Thus, an absolute comparison of scaling exponents in our experiment is uncertain. Nonetheless, our experiments

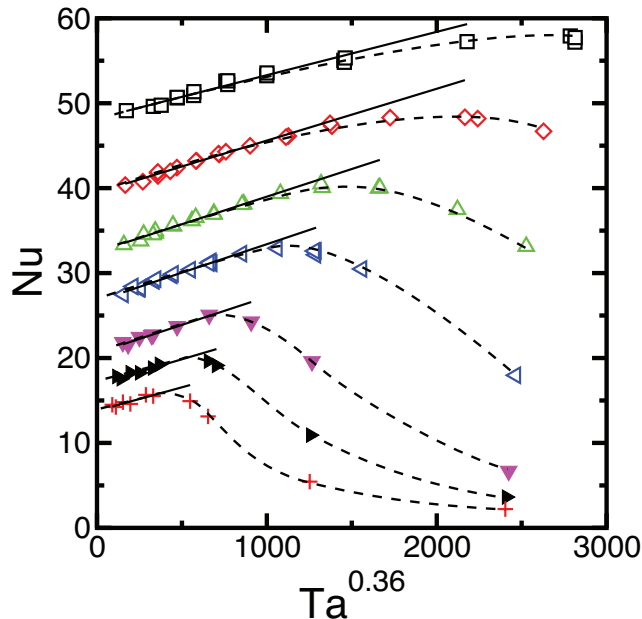


FIG. 8: (Color online) Nu vs $Ta^{0.36}$ so that least-squared fits (solid lines) of $Nu = a Ta^{0.355}$ yield straight lines. From top to bottom, $Ra = 4.0 \times 10^8$, 2.0×10^8 , 1.0×10^8 , 5.0×10^7 , 2.0×10^7 , 1.0×10^7 , and 5.0×10^6 . The dashed lines are guides to the eye and show deviation from linear fit.

yielded some interesting results, especially when compared to numerical simulations [13, 14]. First, at fixed Ro , Nu depends on Ra with a power law close to $2/7$, in agreement with numerical simulation [14] for $Ro = 0.75$ and $\sigma = 1$. If anything, rotation seems to reduce the scaling exponent slightly. This could be the result of different scaling ranges as a function of Ro , because fixed Ro does not exactly maintain a balance between buoyancy and rotation, or because rotation modifies the scaling exponent directly. An extended range in Ra would be necessary to resolve this quantitatively, perhaps in a gas system.

From the perspective of turbulent convection theory [23, 25, 35], the insensitivity of the scaling to rotation is rather interesting because rotation affects many properties of the turbulence, such as the change from thermal plumes to vortices and the existence of a turbulent Eckman boundary layer and associated Eckman pumping. In non-rotating convection, the relationship between the thermal boundary layer thickness δ_T and the viscous sublayer thickness δ_ν determines the power-law scaling in the sheared boundary layer theory [25] where $Nu \sim Ra^{2/7}$ applies when $\delta_T < \delta_\nu$. Rotation introduces another vertical length scale, the Ekman layer thickness δ_E , which could in principle play a role similar to δ_ν in non-rotating convection.

In Fig. 12, we plot δ_T and δ_E as functions of Ra at $Ro = 0.30, 0.75, 1.49$ where δ_T and δ_E are defined as

$$\delta_T = \frac{1}{2} \frac{d}{Nu} \quad (5)$$

$$\delta_E = \left(\frac{\nu}{2\Omega_D} \right)^{1/2} = \frac{d}{Ta^{1/4}} \quad (6)$$

Numerical simulations [13] showed that the transition to turbulent scaling occurs at $Ra \approx 4 \times 10^7$ for $Ro = 0.75$ where $\delta_T \approx \delta_E$. In our experiment we also have $\delta_T \approx \delta_E$ at $Ro = 0.75$ despite the different Prandtl number used in the experiment. Thus, the condition $\delta_T \approx \delta_E$ for a turbulence transition is not consistent with our experiments. It is also interesting to notice that at high $Ra \gg 10^8$ and constant Ro , $\delta_T \propto Ra^{-2/7}$ decreases faster than $\delta_E \sim Ra^{-1/4}$, therefore δ_T and δ_E cross at high Ra for $Ro < 0.75$ and do not cross at Ra for $Ro > 0.75$. The interplay of these two length scales is as yet not understood nor is it clear that δ_E defined from non-convecting problems with differential rotation is the proper variable to use here. It is perhaps interesting to note that along lines of constant Ro , the ratio δ_T/δ_E is almost constant. A direct measurement of the turbulent Ekman layer in the presence of a thermal boundary layer would be very useful to augment the arguments based on numerical simulations [13] for a coexisting thermal

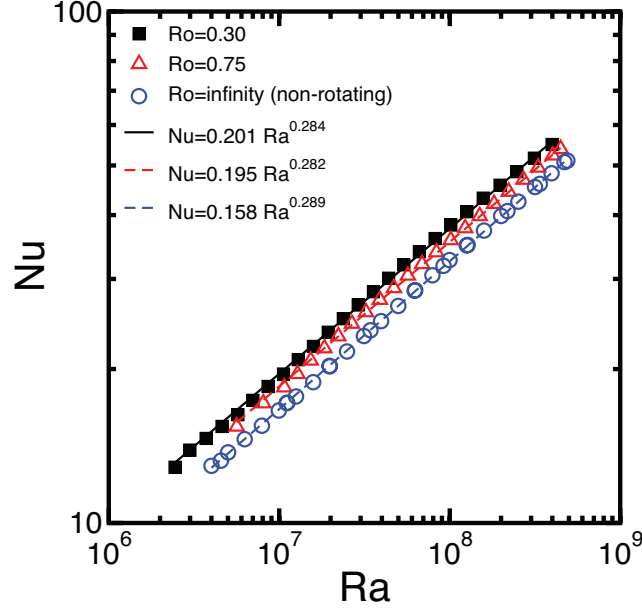


FIG. 9: (Color online) Nu vs Ra at constant Ro: 0.30(■), 0.75(△), and infinity(○). The dashed lines are power-law fits with amplitudes and exponents listed

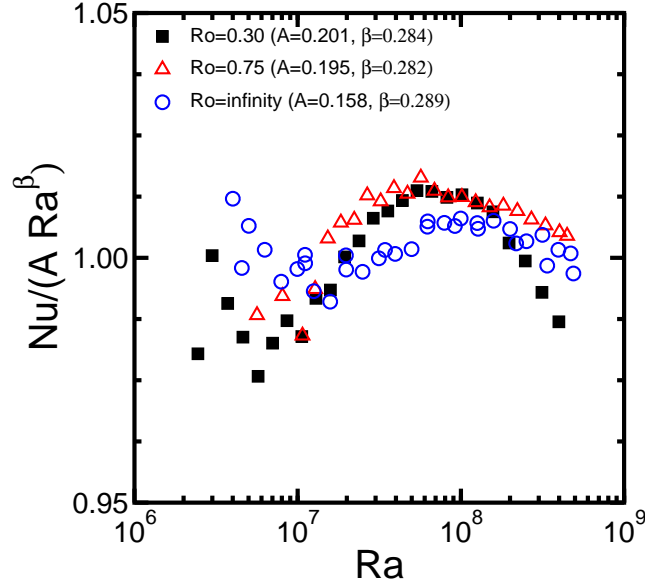


FIG. 10: (Color online) Nu/Ra^β vs Ra at constant Ro: 0.30(■), 0.75(△), and infinity(○, non-rotating).

boundary layer with a linear Ekman layer. Subsequent flow visualization [16] using particle image velocimetry showed an diverse set of interesting behaviors of velocity and vorticity fluctuations but could not yield a definitive conclusion regarding the complex interplay of thermal and kinetic boundary layers involved in determining heat transport for turbulent convection.

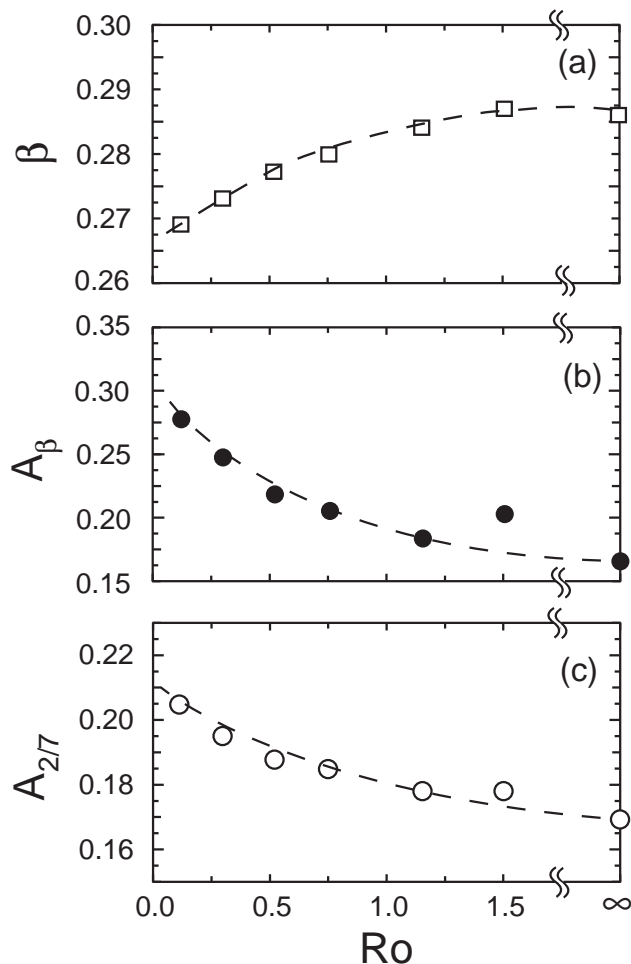


FIG. 11: Rotation-dependence of the fitting parameters: (a) β and (b) A_β in $Nu = A_\beta Ra^\beta$, and (c) coefficient $A_{2/7}$ in $Nu = A_{2/7} Ra^{2/7}$. Dashed lines are guides to the eye.

V. CONCLUSIONS

We have presented experimental studies of turbulent thermal convection in water confined in a cell with a square cross section with and without rotation. In non-rotating convection, the Nusselt number was found to scale roughly as $Ra^{2/7}$ at $4 \times 10^6 < Ra < 5 \times 10^8$. Heat transport measurement in rotating convection confirmed the findings by other researchers [8, 9] that rotation enhances thermal transport over a certain range of Ra and Ta range. Evidence showed that such enhancement may be attributed to the increased effective horizontal area caused by the presence of vortices under rotation. At fixed Rossby number, Nu was found to scale approximately as $Ra^{2/7}$, as does Nu of non-rotating convection and predicted from numerical simulation [14]. Characterization by a combination of power laws [23, 24] was equally good at fitting the data for both rotating and non-rotating convection.

Analysis using Ekman layers instead of kinetic boundary layers as input into a scaling theory did not provide additional insight into the heat transport data, and it remains unclear how rotation and its associated modification of boundary layer structure affects heat transport. Given the extensive study of non-rotating convection in recent years with great advances in characterizing boundary layers, heat transport and large scale circulation [5], there seems to be an emerging opportunity to apply similar rigor to the geophysically important case of rotating thermal convection. We hope that our work may stimulate more experimental and theoretical studies on rotating thermal turbulence. A rigorous test of the power-law scaling of Nu under constant Ro and the validity of Ro as the 'good' parameter requires a much larger Ra and Ta range than what was available in our experiment. A gas convection may be needed to achieve such experimental conditions. The interplay amongst various length scales, such as horizontal vortex wavelength, Ekman layer, thermal boundary layer, viscous sublayer, was not well understood in our experiment and certainly calls for further work on this aspect of turbulent convection.

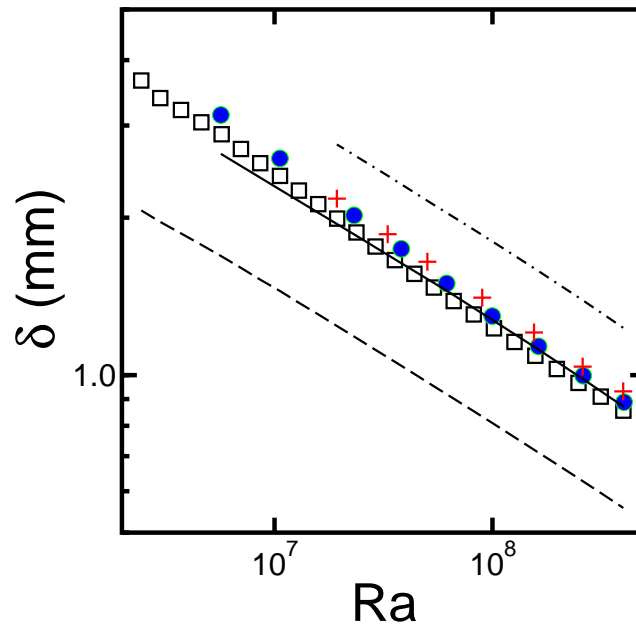


FIG. 12: (Color online) Calculated thermal boundary layer thickness (δ_T , symbols) and Ekman layer thickness (δ_E , lines) at $Ro=0.30$ (\square , dashed line), 0.75 (\bullet , solid line), and 1.49 ($+$, dotted-dashed line).

Acknowledgments

We would like to thank Joe Werne, Keith Julien, Peter Vorobieff, Phil Marcus for helpful discussions. This work was supported by the U.S. Department of Energy.

† Present Address: Jet Propulsion Laboratory, California Institute of Technology, 4800 Oak Grove Drive, MS 79-24, Pasadena, CA 91109

-
- [1] T. Gerkema, J. Zimmerman, L. Maas, and H. van Haren, *Rev. Geophys.* **46** (2008).
 - [2] E. Siggia, *Annu. Rev. Fluid Mech* **26**, 137 (1994).
 - [3] M. Miesch, A. Brun, M. DeRosa, and J. Toomre, *Astrophys. J.* **673**, 557 (2008).
 - [4] J. Aurnou, M. Heimpel, L. Allen, E. King, and J. Wicht, *Geophys. J. Int.* **173**, 793 (2008).
 - [5] G. Ahlers, S. Grossman, and D. Lohse, *Rev. Mod. Phys.* **00**, 00 (2008).
 - [6] S. Chandrasekhar, *Proc. Roy. Soc. London A* **217**, 306 (1953).
 - [7] S. Chandrasekhar (Oxford University Press, Oxford, 1961).
 - [8] H. T. Rossby, *J. Fluid Mech.* **36**, 309 (1969).
 - [9] F. Zhong, R. E. Ecke, and V. Steinberg, *J. Fluid Mech.* **249**, 135 (1993).
 - [10] S. Raasch and D. Etling, *Contrib. Atmos. Phys.* **3**, 1 (1991).
 - [11] W. Cabot, O. Hubickyl, J. Pollack, P. Cassen, and V. Canuto, *Geophys. Astrophys. Fluid Dyn.* **53**, 1 (1990).
 - [12] B. A. Klinger and J. Marshall, *Dyn. Atmos. Oceans* **21**, 227 (1995).
 - [13] K. Julien, S. Legg, J. McWilliams, and J. Werne, *J. Fluid Mech.* **322**, 243 (1996).
 - [14] K. Julien, S. Legg, J. McWilliams, and J. Werne, *Phys. Rev. E* **53**, 5557 (1996).
 - [15] Y. Liu and R. Ecke, *Phys. Rev. Lett.* **79**, 2257 (1997).
 - [16] P. Vorobieff and R. Ecke, *J. Fluid Mech.* **458**, 191 (2002).
 - [17] P. A. Gilman, *Geophys. Astrophys. Fluid Dyn.* **8**, 93 (1977).
 - [18] H. Fernando, R. R. Chen, and D. Boyer, *J. Fluid Mech.* **228**, 513 (1991).
 - [19] H. Jones and J. Marshall, *J. Phys. Oceanogr.* **23**, 1009 (1993).
 - [20] W. Malkus, *Proc. R. Soc. London A* **225**, 196 (1954).
 - [21] L. Howard, in *Applied Mechanics, Proc. 11th Intl. Congr. of Applied Mechanics, Munich (Germany)*, edited by H. Gortler (Springer, Berlin, 1966), p. 1109.

- [22] R. Kraichnan, *Phys. Fluids* **5**, 1374 (1962).
- [23] S. Grossman and D. Lohse, *J. Fluid Mech.* **407**, 27 (2000).
- [24] S. Grossman and D. Lohse, *Phys. Rev. E* **66**, 016305 (2002).
- [25] B. I. Shraiman and E. Siggia, *Phys. Rev. A* **42**, 3650 (1990).
- [26] X. Xu, K. Bajaj, and G. Ahlers, *Phys. Rev. Lett.* **84**, 4357 (2000).
- [27] A. Nikolaenko and G. Ahlers, *Phys. Rev. Lett.* **91**, 084501 (2003).
- [28] J. M. Pfotenhauer, J. J. Niemela, and R. J. Donnelly, *J. Fluid Mech.* **175**, 85 (1987).
- [29] J. C. Buell and I. Catton, *Phys. Fluids* **26**, 892 (1983).
- [30] F. Zhong, R. E. Ecke, and V. Steinberg, *Phys. Rev. Lett.* **67**, 2473 (1991).
- [31] B. M. Boubnov and G. S. Golitsyn, *J. Fluid Mech.* **167**, 503 (1986).
- [32] B. M. Boubnov and G. S. Golitsyn, *J. Fluid Mech.* **219**, 215 (1990).
- [33] L. Ning and R. E. Ecke, *Phys. Rev. E* **47**, 3326 (1993).
- [34] G. Ahlers, *Phys. Rev. E* **63**, 015303 (2000).
- [35] B. Castaing, G. Gunaratne, F. Heslot, L. Kadanoff, A. Libchaber, S. Thomae, X.-Z. Wu, S. Zaleski, and G. Zanetti, *J. Fluid Mech.* **204**, 1 (1989).
- [36] T. H. Solomon and J. P. Gollub, *Phys. Rev. A* **43**, 6683 (1991).
- [37] H. Tanaka and H. Miyata, *J. Heat Mass Transfer* **23**, 1273 (1980).
- [38] G. Zocchi, E. Moses, and A. Libchaber, *Physica A* **166**, 387 (1990).
- [39] J. Hart, S. Kittelman, and D. Ohlsen, *Phys. Fluids* **14**, 955 (2002).
- [40] R. Kunnen, H. Clercx, and B. Geurts, *Europhys. Lett.* **84**, 24001 (2008).
- [41] S. Sakai, *J. Fluid Mech.* **333**, 85 (1997).